

Binary-pulsar tests of strong-field gravity*

Gilles Esposito-Farèse

*Centre de Physique Théorique[†], CNRS Luminy
Case 907, F 13288 Marseille Cedex 9, France*

(December 16, 1996)

Abstract

This talk is based on my work in collaboration with Thibault Damour since 1991. Unified theories, like superstrings, predict the existence of scalar partners to the graviton. Such theories of gravity can be very close to general relativity in weak-field conditions (solar-system experiments), but can deviate significantly from it in the strong-field regime (near compact bodies, like neutron stars). Binary pulsars are thus the best tools available for testing these theories. This talk presents the four main binary-pulsar experiments, and discusses the constraints they impose on a generic class of tensor-scalar theories. It is shown notably that they rule out some models which are strictly indistinguishable from general relativity in the solar system. This illustrates the qualitative difference between binary-pulsar and solar-system tests of relativistic gravity.

CPT-96/P.3411
gr-qc/9612039

*To appear in: *Pulsar Timing, General Relativity, and the Internal Structure of Neutron Stars*, Proceedings of a Colloquium held at the Royal Netherlands Academy of Arts and Sciences, 24–28 September, 1996.

[†]Unité Propre de Recherche 7061.

1 Introduction

The usual meaning of “testing a theory” is rather negative: One compares its predictions with experimental data, and a single inconsistency suffices to rule it out. On the other hand, it is difficult to determine what features of the theory are correct when it passes a given test. In order to extract some positive information from experiment, it is useful to embed the theory into a class of alternatives. Indeed, by contrasting their predictions, it is easier to understand in what way they differ, and to determine the common features which make them pass or not the available tests. Moreover, this approach can suggest new experiments to test the other features of the theories.

The best known example of such an embedding of general relativity into a space of alternatives is the so-called Parametrized Post-Newtonian (PPN) formalism, which is extremely useful for studying gravity in weak-field conditions, at order $1/c^2$ with respect to the Newtonian interaction. The original idea was formulated by Eddington [1], who wrote the usual Schwarzschild metric in isotropic coordinates, but introduced some phenomenological parameters β^{PPN} , γ^{PPN} , in front of the different powers of the dimensionless ratio Gm/rc^2 :

$$-g_{00} = 1 - 2\frac{Gm}{rc^2} + 2\beta^{\text{PPN}} \left(\frac{Gm}{rc^2}\right)^2 + O\left(\frac{1}{c^6}\right) , \quad (1a)$$

$$g_{ij} = \delta_{ij} \left[1 + 2\gamma^{\text{PPN}} \frac{Gm}{rc^2} + O\left(\frac{1}{c^4}\right) \right] . \quad (1b)$$

General relativity, which corresponds to $\beta^{\text{PPN}} = \gamma^{\text{PPN}} = 1$, is thus embedded into a two-dimensional space of theories parametrized by all real values of β^{PPN} , γ^{PPN} . [The third parameter that one may introduce in front of $2Gm/rc^2$ in g_{00} can be reabsorbed in the definition of the mass m .]

The constraints imposed in this space by solar-system experiments are displayed in Fig. 1, and give the following 1σ limits on the Eddington parameters:

$$|\beta^{\text{PPN}} - 1| < 6 \times 10^{-4} , \quad (2a)$$

$$|\gamma^{\text{PPN}} - 1| < 2 \times 10^{-3} . \quad (2b)$$

The PPN formalism has been further developed by Schiff, Baierlin, Nordtvedt and Will to describe any possible relativistic theory of gravity at order $1/c^2$. In particular, Will and Nordtvedt [2] introduced up to 8 extra parameters (besides β^{PPN} and γ^{PPN}), each of them describing a particular violation of

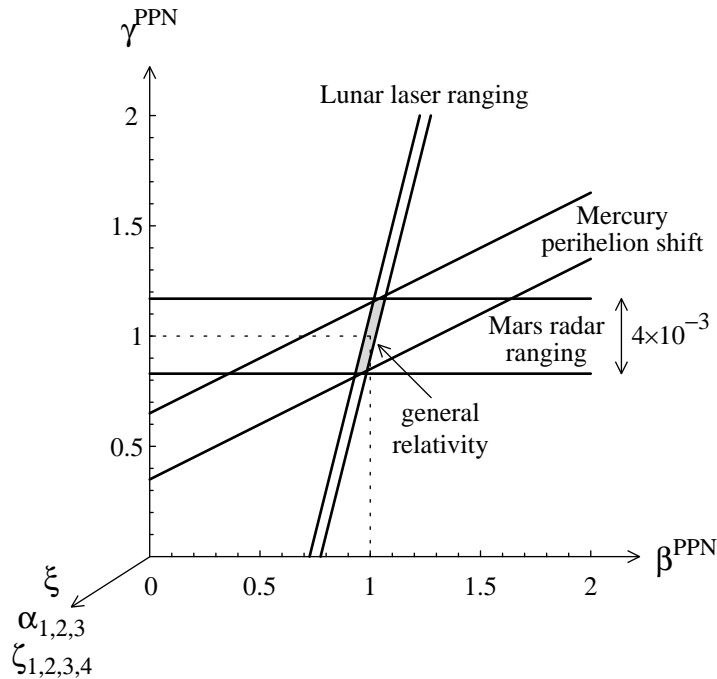


Figure 1: Solar-system constraints on the PPN parameters. The widths of the strips have been enlarged by a factor 100. The allowed region is shaded.

the symmetries of general relativity, like local Lorentz invariance, or the conservation of energy and momentum. Since these 8 parameters do not have any really natural field-theoretic motivation (as opposed to β^{PPN} and γ^{PPN} ; see below), we will not consider them any longer in this paper. Let us just mention that they are even more constrained than $(\beta^{\text{PPN}} - 1)$ and $(\gamma^{\text{PPN}} - 1)$ by solar-system experiments. [See the contribution of J. Bell to the present Proceedings for a discussion of the tight bounds on some of these parameters imposed by binary-pulsar data.] In the 10-dimensional space of all these PPN parameters (β^{PPN} , γ^{PPN} , and the 8 others), only a tiny neighborhood of Einstein's theory is thus allowed by solar-system experiments: the intersection of the three strips of Fig. 1 and a very thin 8-dimensional slice parallel to the plane of this Figure. One can therefore conclude that general relativity is essentially the only theory which passes all these tests, and one may naturally ask the question: Is it worth testing it any further ?

The reason why solar-system tests do not suffice is the extreme weakness of the gravitational field in these conditions. Indeed, the largest deviation from the flat metric is found at the surface of the Sun, and is proportional

to its gravitational binding energy $(Gm/Rc^2)_{\odot} \approx 2 \times 10^{-6}$ (where R denotes the radius of the considered body). In the vicinity of the Earth, the gravitational field is of order $(Gm/Rc^2)_{\oplus} \approx 7 \times 10^{-10}$. This explains why only the first terms of the expansion (1) are tested by solar-system experiments. Two theories which are extremely close in weak-field conditions can differ significantly in the strong-field regime. For instance, the typical self-energy of a neutron star is $Gm/Rc^2 \approx 0.2$, and therefore one cannot justify any more the PPN truncation of the theory at order $1/c^2$. [A more rigorous definition of the binding energy is $-\partial \ln m / \partial \ln G$. This expression takes its maximum value, 0.5, for black holes. The value ≈ 0.2 found for neutron stars should therefore be understood as a rather *large* number.] Binary pulsars are thus ideal tools for testing relativistic theories of gravity in strong-field conditions.

Before embedding general relativity into a class of contrasting alternatives, and comparing their predictions with experimental data, let us first describe the four main binary-pulsar tests presently available.

2 Binary-pulsar tests

The aim of this talk is not to explain what is a pulsar to specialists of the question. For our purpose, it is sufficient to note that an isolated pulsar is essentially a (very stable) clock. A binary pulsar (a pulsar and a companion orbiting around each other) is thus a *moving clock*, the best tool that one could dream of to test a relativistic theory. Indeed, the frequency of the pulses is modified by the motion of the pulsar (Doppler effect), and one can extract from the Table Of Arrivals many information concerning the orbit. For instance, the orbital period P_b can be obtained from the time between two maxima of the pulse frequency. One can also measure several other Keplerian parameters, like the eccentricity e of the orbit, the angular position ω of the periastron, etc.

In the case of PSR B 1913+16, which has been continuously observed since its discovery in 1974 [3], the data are so precise that one can even measure three relativistic effects with great accuracy. (i) The redshift due to the companion¹ $\propto Gm_B/r_{AB}c^2$ and the second-order Doppler effect $\propto v_A^2/2c^2$ are combined in an observable which has been denoted γ_{Timing} . [The index ‘‘Timing’’ is written to avoid a confusion with the Eddington parameter γ^{PPN} introduced in Eq. (1b).] Since the Keplerian parameters P_b and ω have been measured accurately during two decades, their time derivatives are also available: (ii) $\dot{\omega}$ gives the periastron advance (a relativistic effect of order v^2/c^2),

¹ A denotes the pulsar, B the companion, and r_{AB} the distance between them.

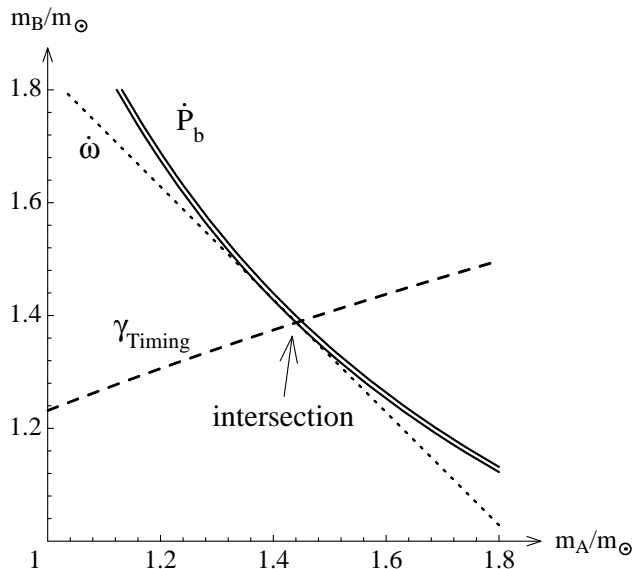


Figure 2: General relativity passes the $(\gamma_{\text{Timing}}-\dot{\omega}-\dot{P}_b)_{1913+16}$ test.

and (iii) the variation of the orbital period, \dot{P}_b , can be interpreted as a consequence of the energy loss due to the emission of gravitational waves (an effect of order v^5/c^5 in general relativity, but generically of order v^3/c^3 in alternative theories; see below). The three “post-Keplerian” observables γ_{Timing} , $\dot{\omega}$, \dot{P}_b can thus be compared with the predictions of a given theory, which depend on the unknown masses m_A , m_B of the pulsar and its companion. However, 3 observables minus 2 unknown quantities is still 1 test. The equations $\gamma_{\text{Timing}}^{\text{th}}(m_A, m_B) = \gamma_{\text{Timing}}^{\text{obs}}$, $\dot{\omega}^{\text{th}}(m_A, m_B) = \dot{\omega}^{\text{obs}}$, $\dot{P}_b^{\text{th}}(m_A, m_B) = \dot{P}_b^{\text{obs}}$, define three curves (in fact three *strips*) in the two-dimensional plane of the masses (m_A, m_B) . If the three strips meet in a small region, there exists a pair of masses (m_A, m_B) which is consistent with all three observables, and therefore the theory is consistent with the binary-pulsar data. If they do not meet, the theory is ruled out. Figure 2 displays these strips in the case of general relativity, which passes the test with flying colors. [We will see below that some other theories can also pass this test.]

The binary pulsar PSR B 1534+12 has been observed only since 1991 [4] but it is much closer to the Earth than PSR B 1913+16, and three post-Keplerian observables have already been measured with good precision: γ_{Timing} , $\dot{\omega}$, and a new parameter denoted s . It is involved in the shape of the Shapiro time delay (an effect $\propto 1/c^3$ due to the propagation of light in the curved spacetime around the companion), and it can be interpreted as the

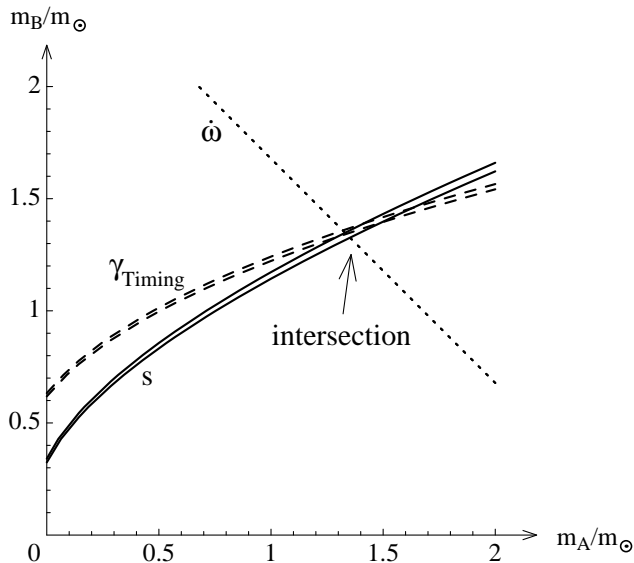


Figure 3: General relativity passes the $(\gamma_{\text{Timing}} - \dot{\omega} - s)_{1534+12}$ test.

sine $s = \sin i$ of the angle between the orbit and the plane of the sky. [The range r of this Shapiro time delay is also measured but with less precision.] Here again, the three strips “predictionsth $(m_A, m_B) = \text{observed values}$ ” can be plotted for a given theory, and if they meet each other, the test is passed. Figure 3 displays the case of general relativity, which passes the test at the 1σ level [5].

As shown in Sec. 3 below, generic theories of gravity predict a large dipolar emission of gravitational waves (of order v^3/c^3) when the masses of the pulsar and its companion are very different, whereas the prediction of general relativity starts at the much weaker quadrupolar order ($\propto v^5/c^5$). Several dissymmetrical systems, like the neutron star–white dwarf binary PSR B 0655+64, happen to have very small observed values of \dot{P}_b , consistent with general relativity but not with a typical dipolar radiation. This is the third binary-pulsar test that we will use to constrain the space of gravity theories.

We will also see in Sec. 3 below that in generic theories of gravity, the acceleration of a neutron star towards the center of the Galaxy is not the same as the acceleration of a white dwarf. This violation of the strong equivalence principle causes a “gravitational Stark effect” on the orbit of a neutron star–white dwarf system: Its periastron is polarized towards the center of the Galaxy. [This is similar to the effects discussed in J. Bell’s contribution to

the present Proceedings.] More precisely, the eccentricity vector \mathbf{e} of the orbit is the sum of a fixed vector \mathbf{e}_F directed towards the Galaxy center (proportional to the difference of the accelerations of the bodies), and of a rotating vector $\mathbf{e}_R(t)$ corresponding to the usual periastron advance at angular velocity $\dot{\omega}_R$. Several dissymmetrical systems of this kind (such as PSRs 1855+09, 1953+29, 1800–27) happen to have a very small eccentricity. The only explanation would be that the rotating vector $\mathbf{e}_R(t)$ is precisely canceling the fixed contribution \mathbf{e}_F at the time of our observation: $\mathbf{e}_F + \mathbf{e}_R(t) \approx \mathbf{0}$. However, this is very improbable, and one can use a statistical argument to constrain the space of theories [6]. Moreover, by considering several such systems, the probability that they have simultaneously a small eccentricity is the product of the already small individual probabilities. This idea has been used in [7] to derive a very tight bound on the difference of the accelerations of the bodies. This is the fourth binary-pulsar test that we will use in the following. Of course, general relativity passes this test, since it does satisfy the strong equivalence principle (universality of free fall of self-gravitating objects).

These four tests are presently the most precise of all those which are available. It should be noted that many other tests are *a priori* possible: Damour and Taylor [8] have shown that 15 tests are in principle possible for each binary pulsar, if the pulses are measured precisely enough.

3 Tensor-scalar theories of gravity

3.1 Introduction and action

We saw in the previous section that several tests of gravity can be performed in the strong-field regime, and that general relativity passes all of them. As discussed in Sec. 1, our aim is now to embed Einstein’s theory into a class of alternatives, in order to determine what features have been tested, and what can be further tested. A generalization of the PPN formalism to all orders in $1/c^n$ would need an infinite number of parameters [cf. Eq. (1)]. We will instead focus on the most natural class of alternatives to general relativity: “tensor-scalar” theories, in which gravity is mediated by a tensor field ($g_{\mu\nu}$) and one or several scalar fields (φ). Here are the main reasons why this class is privileged. (i) Scalar partners to the graviton arise naturally in theoretical attempts at quantizing gravity or at unifying it with other interactions (superstrings, Kaluza-Klein). (ii) They are the only consistent massless field theories able to satisfy the weak equivalence principle (universality of free fall of laboratory-size objects). (iii) They are the only known theories satisfying

“extended Lorentz invariance” [9], *i.e.*, such that the physics of subsystems, influenced by external masses, exhibit Lorentz invariance. (iv) They explain the key role played by β^{PPN} and γ^{PPN} in the PPN formalism (the extra 8 parameters quoted in the Introduction vanish identically in tensor-scalar theories). (v) They are general enough to describe many different deviations from general relativity, but simple enough for their predictions to be fully worked out [10].

Like in general relativity, the action of matter is given by a functional $S_m[\psi_m, \tilde{g}_{\mu\nu}]$ of some matter fields ψ_m (including gauge bosons) and one second-rank symmetric tensor² $\tilde{g}_{\mu\nu}$. The difference with general relativity lies in the kinetic term of $\tilde{g}_{\mu\nu}$. Instead of being a pure spin-2 field, it is here a mixing of spin-2 and spin-0 excitations. More precisely, it can be written as $\tilde{g}_{\mu\nu} = \exp[2a(\varphi)]g_{\mu\nu}$, where $a(\varphi)$ is a function of a scalar field φ , and $g_{\mu\nu}$ is the Einstein (spin 2) metric. The action of the theory reads thus

$$S = \frac{c^3}{16\pi G} \int d^4x \sqrt{-g} (R - 2g^{\mu\nu} \partial_\mu \varphi \partial_\nu \varphi) + S_m [\psi_m, e^{2a(\varphi)} g_{\mu\nu}] . \quad (3)$$

[Our signature is $-+++$, R is the scalar curvature of $g_{\mu\nu}$, and g its determinant.]

Our discussion will now be focused on the function $a(\varphi)$, which characterizes the coupling of matter to the scalar field. It will be convenient to expand it around the background value φ_0 of the scalar field (*i.e.*, its value far from any massive body):

$$a(\varphi) = \alpha_0(\varphi - \varphi_0) + \frac{1}{2}\beta_0(\varphi - \varphi_0)^2 + \frac{1}{3!}\beta'_0(\varphi - \varphi_0)^3 + \dots , \quad (4)$$

where α_0 , β_0 , β'_0 , \dots are constants defining the theory. General relativity corresponds to a vanishing function $a(\varphi) = 0$, and Jordan-Fierz-Brans-Dicke theory to a linear function $a(\varphi) = \alpha_0(\varphi - \varphi_0)$. We will see in Sec. 5 below that interesting strong-field effects occur when $\beta_0 \neq 0$, *i.e.*, when $a(\varphi)$ has a nonvanishing curvature.

3.2 Weak-field constraints

Before studying the behavior of these theories in strong-field conditions, it is necessary to take into account the solar-system constraints (2). A simple diagrammatic argument [11] allows us to derive the expressions of the effective gravitational constant between two bodies, and of the Eddington PPN

²To simplify, we will consider here only theories which satisfy exactly the weak equivalence principle, and we will restrict our discussion to a single scalar field except in Sec. 4.

parameters in tensor-scalar theories:

$$G^{\text{eff}} = G(1 + \alpha_0^2), \quad (5a)$$

$$\gamma^{\text{PPN}} - 1 = -2\alpha_0^2/(1 + \alpha_0^2), \quad (5b)$$

$$\beta^{\text{PPN}} - 1 = \frac{1}{2} \frac{\alpha_0 \beta_0 \alpha_0}{(1 + \alpha_0^2)^2}. \quad (5c)$$

[The factor α_0^2 comes from the exchange of a scalar particle between two bodies, whereas $\alpha_0 \beta_0 \alpha_0$ comes from a scalar exchange between three bodies.] The bounds (2) can therefore be rewritten as

$$\alpha_0^2 < 10^{-3}, \quad (6a)$$

$$|\alpha_0^2 \beta_0| < 1.2 \times 10^{-3}. \quad (6b)$$

The first equation tells us that the slope of the function $a(\varphi)$ cannot be too large: The scalar field is linearly *weakly* coupled to matter. The second equation does not tell us much, since we already know that α_0^2 is small. In particular, it does not tell us if β_0 is positive [$a(\varphi)$ convex] or negative [$a(\varphi)$ concave].

The same diagrammatic argument can also be used to show that any deviation from general relativity at order $1/c^n$ ($n \geq 2$) involves at least two factors α_0 , and has the schematic form

$$\text{deviation from G.R.} = \alpha_0^2 \times \left[\lambda_0 + \lambda_1 \frac{Gm}{Rc^2} + \lambda_2 \left(\frac{Gm}{Rc^2} \right)^2 + \dots \right], \quad (7)$$

where Gm/Rc^2 is the compactness of a body, and $\lambda_0, \lambda_1, \dots$ are constants built from the coefficients $\alpha_0, \beta_0, \beta'_0, \dots$ of expansion (4). Since α_0^2 is known to be small, we thus expect the theory to be close to general relativity at any order. [We do not wish to consider models involving unnaturally large dimensionless numbers in the expansions (4) or (7).] However, in two different cases that will be discussed in Sections 4 and 5, the theory can exhibit significant strong-field deviations from general relativity: (i) If the theory involves more than one scalar field, Eq. (6a) does not necessarily imply that the slope of $a(\varphi)$ is small. (ii) Some nonperturbative effects can develop in strong-field conditions, and the sum of the series in the square brackets of Eq. (7) can be large enough to compensate even a vanishingly small α_0^2 .

3.3 Strong-field predictions

The predictions of tensor-scalar theories in strong-field conditions have been derived in [10]. They mimic the weak-field predictions with the important

difference that the constants α_0, β_0 must be replaced by body-dependent parameters $\alpha_A \equiv \partial \ln m_A / \partial \varphi_0$, $\beta_A \equiv \partial \alpha_A / \partial \varphi_0$ (and similarly for the companion B). These parameters can be interpreted essentially as the slope and the curvature of $a(\varphi)$ at the center of body A (or body B). [In the weak-field regime, one has $\varphi \approx \varphi_0$, therefore $\alpha_A \approx \alpha_0$, $\beta_A \approx \beta_0$.] In particular, the effective gravitational constant between two self-gravitating bodies A and B reads

$$G_{AB}^{\text{eff}} = G(1 + \alpha_A \alpha_B), \quad (8)$$

instead of (5a). The acceleration of a neutron star A towards the center C of the Galaxy is thus proportional to $(1 + \alpha_A \alpha_C)$, whereas a white dwarf B is accelerated with a force $\propto (1 + \alpha_B \alpha_C)$. Since $\alpha_A \neq \alpha_B$ in general, there is a violation of the strong equivalence principle which causes the ‘‘gravitational Stark effect’’ discussed in Sec. 2.

The strong-field analogues of γ^{PPN} and β^{PPN} are given by formulas similar to (5b), (5c), but α_0^2 is replaced by $\alpha_A \alpha_B$ and $\alpha_0 \beta_0 \alpha_0$ by a combination of $\alpha_A \beta_B \alpha_A$ and $\alpha_B \beta_A \alpha_B$. The prediction for the periastron advance $\dot{\omega}$ can thus be written straightforwardly.

The expression of the observable parameter γ_{Timing} involves again the body-dependent parameters α_A, α_B , but also a subtle contribution proportional to $\alpha_B \times \partial \ln I_A / \partial \varphi_0$, where I_A is the inertia moment of the pulsar. This term is due to the modification of the equilibrium configuration of the pulsar due to the presence of its companion at a varying distance. We have shown in [12] how to compute this effect, which happens to be particularly large in some models (see Sec. 5 below).

The energy flux carried out by gravitational waves has been computed in [10]. It is of the form

$$\begin{aligned} \text{Energy flux} = & \left\{ \frac{\text{Quadrupole}}{c^5} + O\left(\frac{1}{c^7}\right) \right\}_{\text{helicity } 2} \\ & + \left\{ \frac{\text{Monopole}}{c} + \frac{\text{Dipole}}{c^3} + \frac{\text{Quadrupole}}{c^5} + O\left(\frac{1}{c^7}\right) \right\}_{\text{helicity } 0}. \end{aligned} \quad (9)$$

The first curly brackets contain the prediction of general relativity. The second ones contain the extra terms predicted in tensor-scalar theories. The powers of $1/c$ give the orders of magnitude of the different terms. In particular, the monopolar and dipolar helicity-0 waves are generically expected to be much larger than the usual quadrupole of general relativity. However, the scalar monopole has the form

$$\frac{\text{Monopole}}{c} = \frac{G}{c} \left\{ \frac{\partial(m_A \alpha_A)}{\partial t} + \frac{\partial(m_B \alpha_B)}{\partial t} + O\left(\frac{1}{c^2}\right) \right\}^2, \quad (10)$$

and it reduces to order $O(1/c^5)$ if the stars A and B are at equilibrium [$\partial_t(m_A\alpha_A) = 0$], which is the case for all binary pulsars quoted in Sec. 2. [It should be noted, however, that this monopole would be huge in the case of a collapsing star, for instance.] The dipole has the form

$$\frac{\text{Dipole}}{c^3} = \frac{G}{3c^3} \left(\frac{G_{AB}^{\text{eff}} m_A m_B}{r_{AB}^2} \right)^2 (\alpha_A - \alpha_B)^2 + O\left(\frac{1}{c^5}\right), \quad (11)$$

and is usually much larger than a quadrupole of order $1/c^5$ (see the third test discussed in Sec. 2). However, when the two stars A and B are very similar (e.g. two neutron stars), one has $\alpha_A \approx \alpha_B$ and this dipolar contribution almost vanishes. [A dipole is a vector in space; two identical stars do not define a preferred orientation.]

4 Tensor-multi-scalar theories

In order to satisfy the weak-field constraints (6) but still predict significant deviations from general relativity in the strong-field regime, the first possibility is to consider tensor-scalar theories involving at least two scalar fields [10]. Indeed, there can exist an exact compensation between the two fields in the solar system, although both of them can be strongly coupled to matter. If the kinetic terms of the scalar fields read $-(\partial_\mu\varphi_1)^2 + (\partial_\mu\varphi_2)^2$, Eq. (6a) becomes $|\alpha_1^2 - \alpha_2^2| < 10^{-3}$, and none of the coupling constants α_1, α_2 needs to be small. However, one of the fields (here φ_2) must carry negative energy for this compensation to occur. Therefore, these tensor-bi-scalar theories can be considered only as *phenomenological* models, useful as contrasting alternatives to general relativity but with no fundamental significance.

We have constructed in Ref. [10] the simplest tensor-bi-scalar model which has the following properties: (i) It has the same post-Newtonian limit as general relativity ($\beta^{\text{PPN}} = \gamma^{\text{PPN}} = 1$), and therefore passes all solar-system tests. (ii) It does not predict any dipolar radiation $\propto 1/c^3$ [$\forall A, \forall B, (\alpha_A - \alpha_B)^2 = 0$], and therefore passes the third binary-pulsar test discussed in Sec. 2. Moreover, it depends on two parameters, β', β'' , and general relativity corresponds to $\beta' = \beta'' = 0$. Figure 4 displays the constraints imposed by the three other binary-pulsar tests of Sec. 2 in the plane of the parameters (β', β'') . The theories passing the 1913+16 test are inside the long strip plotted in solid lines. Note that theories which are very different from general relativity can pass this test. For instance, Fig. 5 displays the mass plane (m_A, m_B) for the (fine-tuned) model $\beta' = 8, \beta'' = 69$. The three strips are significantly different from those of Fig. 2, but they still meet each other in a small region [corresponding to values of the masses m_A, m_B different from

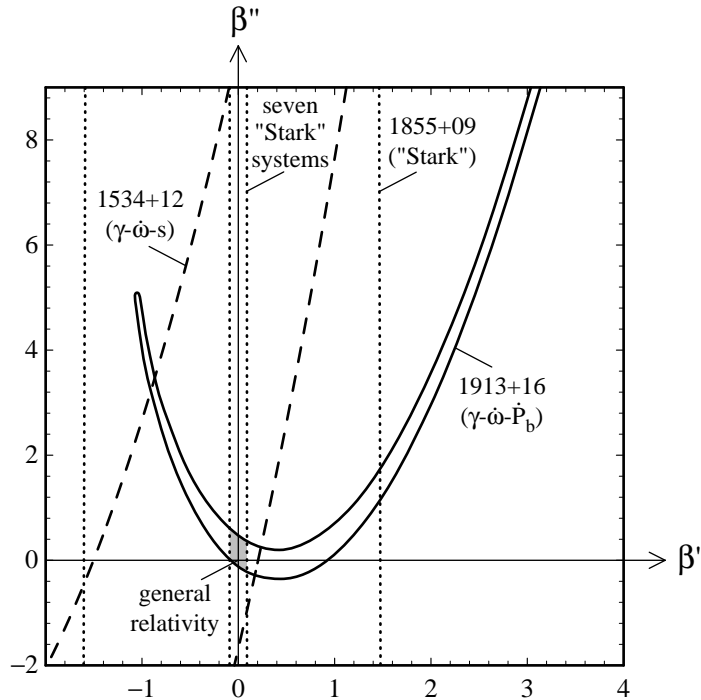


Figure 4: Constraints imposed by the binary-pulsar tests of Sec. 2 on the tensor-bi-scalar model of Sec. 4. The two dotted strips illustrate how the precision of the “Stark” test is increased when several binary pulsars are considered simultaneously. The region allowed by all tests is the small shaded diamond around general relativity ($\beta' = \beta'' = 0$).

those found in general relativity]. To illustrate how much the theory differs from general relativity, let us just mention that the effective gravitational constant G_{AB}^{eff} between the pulsar and its companion is 1.7 times larger than the bare Newtonian constant G . We have thus exhibited a model which deviates by 70 % from Einstein’s theory, but passes (i) all solar-system tests, (ii) the “no-dipolar-radiation” test of PSR 0655+64, and (iii) the “ $\gamma_{\text{Timing}}-\dot{\omega}-\dot{P}_b$ ” test of PSR 1913+16. Before our work, this 1913+16 test was usually considered as enough to rule out any theory but general relativity. We have proven that other binary-pulsar tests are also necessary. In particular, Fig. 4 shows clearly that the “ $\gamma_{\text{Timing}}-\dot{\omega}-s$ ” test of PSR 1534+12 and the “Stark” test complement it usefully. For instance, the model of Fig. 5 is easily ruled out by the 1534+12 test: the γ_{Timing} and s curves do not even meet each other (so that the observable $\dot{\omega}$ is not even useful here).

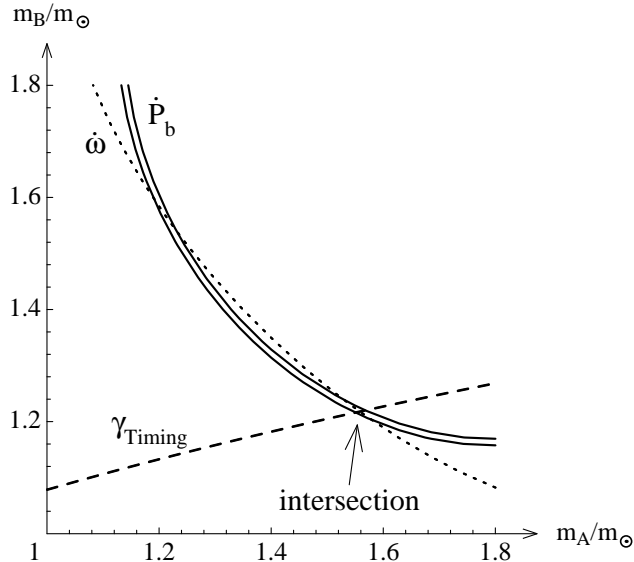


Figure 5: The tensor-bi-scalar model $\beta' = 8$, $\beta'' = 69$, passes the $(\gamma_{\text{Timing}} - \dot{\omega} - \dot{P}_b)_{1913+16}$ test, although the three curves are significantly different from those of Fig. 2.

Thanks to the four binary-pulsar tests discussed in Sec. 2, this class of tensor-bi-scalar models is now essentially ruled out. We have achieved a similar result as in the weak-field regime of Fig. 1: Only a tiny neighborhood of general relativity is still allowed. This is a much stronger result than just verifying that Einstein’s theory passes these four tests.

5 Nonperturbative strong-field effects

We now discuss the second way to satisfy the constraints (6) while predicting significant deviations from general relativity in the strong-field regime. As opposed to the models of the previous section, we consider here well-behaved theories, with only positive-energy excitations (of the type that is predicted by superstrings and extra-dimensional theories). To simplify, we will also restrict our discussion to the case of a single scalar field φ .

The simplest tensor-scalar theory, Jordan-Fierz-Brans-Dicke theory, cannot give rise to nonperturbative strong-field effects for an obvious reason. It corresponds to a linear coupling function $a(\varphi) = \alpha_0(\varphi - \varphi_0)$, and even if the field φ_A at the center of body A is very different from the background φ_0 ,

one has anyway $\alpha_A \approx a'(\varphi_A) = \alpha_0$. Therefore, the deviations from general relativity, proportional to $\alpha_A \alpha_B \approx \alpha_0^2$, are constrained by the solar-system limit (6a) to be $\lesssim 0.1\%$ even in the vicinity of neutron stars.

On the contrary, if we consider a quadratic coupling function $a(\varphi) = \frac{1}{2}\beta_0\varphi^2$, the field equation for φ in a body of constant density ρ is of the form $d^2(r\varphi)/dr^2 \approx \beta_0\rho \cdot (r\varphi)$. Therefore, the solution involves a sinh if $\beta_0 > 0$, and a sin if $\beta_0 < 0$. More precisely, one finds

$$\alpha_A \approx \alpha_0 / \cosh \sqrt{3\beta_0 Gm/Rc^2} \quad \text{if } \beta_0 > 0, \quad (12a)$$

$$\alpha_A \approx \alpha_0 / \cos \sqrt{3|\beta_0|Gm/Rc^2} \quad \text{if } \beta_0 < 0. \quad (12b)$$

In the case of a convex coupling function $a(\varphi)$ (*i.e.*, $\beta_0 > 0$), the deviations from general relativity are thus smaller in strong-field conditions than in the weak-field regime: $\alpha_A \alpha_B < \alpha_0^2 < 10^{-3}$. On the other hand, a concave $a(\varphi)$ can give rise to significant deviations: If $\beta_0 \lesssim -4$, the argument of the cosine function is close to $\pi/2$ for a typical neutron star ($Gm/Rc^2 \approx 0.2$), and α_A can thus be large even if α_0 is vanishingly small. To understand intuitively what happens when $\alpha_0 = 0$ strictly (*i.e.*, when the theory is strictly equivalent to general relativity in weak-field conditions), it is instructive to compute the energy of a typical configuration of the scalar field, starting from a value φ_A at the center of body A and tending towards 0 as $1/r$ outside. One gets a result of the form

$$\text{Energy} \approx \int \left[\frac{1}{2}(\partial_i\varphi)^2 + \rho e^{\beta_0\varphi^2/2} \right] \approx mc^2 \left(\frac{\varphi_A^2/2}{Gm/Rc^2} + e^{\beta_0\varphi_A^2/2} \right). \quad (13)$$

When $\beta_0 < 0$, this is the sum of a parabola and a Gaussian, and if the compactness Gm/Rc^2 is large enough, the function $\text{Energy}(\varphi_A)$ has the shape of a Mexican hat; the value $\varphi_A = 0$ now corresponds to a local *maximum* of the energy. It is therefore energetically favorable for the star to create a nonvanishing scalar field φ_A , and thereby a nonvanishing “scalar charge” $\alpha_A \approx \beta_0\varphi_A$. This phenomenon is analogous to the spontaneous magnetization of ferromagnets.

We have verified the above heuristic arguments by explicit numerical calculations [13], taking into account the coupled differential equations of the metric and the scalar field, and using a realistic equation of state to describe nuclear matter inside a neutron star. We found that there is indeed a “spontaneous scalarization” above a critical mass, whose value depends on β_0 . Figure 6 displays the scalar charge α_A for the model $\beta_0 = -6$. Note that the deviations from general relativity are of order $\alpha_A \alpha_B \approx 35\%$ for a wide range of masses from $\approx 1.25 m_\odot$ to the maximum mass; therefore, no fine

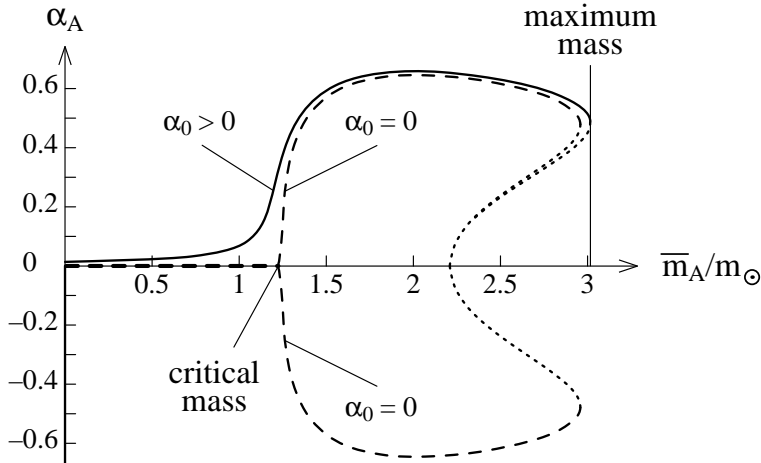


Figure 6: Scalar charge α_A versus baryonic mass \bar{m}_A , for the model $a(\varphi) = -3\varphi^2$ (i.e., $\beta_0 = -6$). The solid line corresponds to the maximum value of α_0 allowed by solar-system experiments, and the dashed lines to $\alpha_0 = 0$ (“zero-mode”). The dotted lines correspond to unstable configurations of the star.

tuning is necessary to get large deviations in a particular binary pulsar. Note also that the nonperturbative effects do not vanish with α_0 : Even if the theory is *strictly* equivalent to general relativity in the solar system, it deviates significantly from it near compact bodies. In fact, an even more surprising phenomenon occurs for the term $\alpha_B \partial \ln I_A / \partial \varphi_0$ involved in the observable γ_{Timing} (see Sec. 2): This term blows up as $\alpha_0 \rightarrow 0$. In other words, a theory which is closer to general relativity in weak-field conditions predicts larger deviations in the strong-field regime!

The “ $\gamma_{\text{Timing}}-\dot{\omega}-\dot{P}_b$ ” test of PSR 1913+16 is displayed in Fig. 7 for the model $\beta_0 = -6$ and the maximum value of α_0 allowed by solar-system experiments. [The “ $\gamma_{\text{Timing}}-\dot{\omega}-s$ ” test of PSR 1534+12 gives curves similar to those of Fig. 7 for the first two observables, while the s strip is only slightly deviated from that of Fig. 3.] The great deformation of the \dot{P}_b curve, as compared to the general relativistic prediction, Fig. 2, is due to the emission of dipolar waves in tensor-scalar theories. The fact that this dipolar radiation vanishes on the diagonal $m_A = m_B$ explains the shape of this curve. As expected, the γ_{Timing} curve is also very deformed because of the contribution $\alpha_B \partial \ln I_A / \partial \varphi_0$. When β_0 is not too negative (e.g. $\beta_0 \approx -4$), a smaller value of α_0 allows the test to be passed: the three curves finally meet in one point.

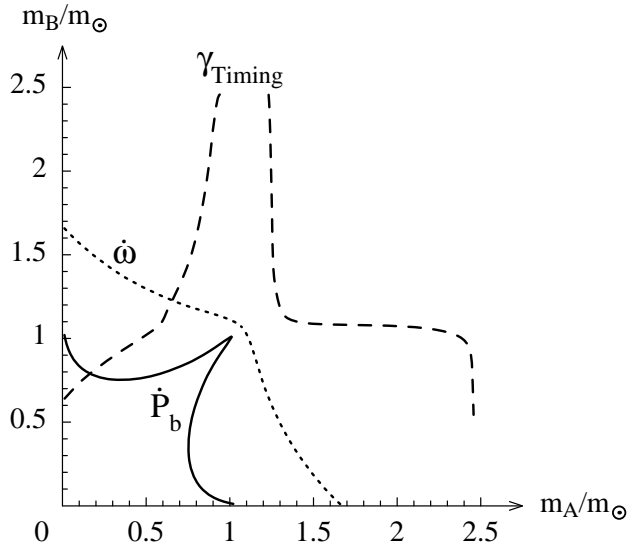


Figure 7: The model $a(\varphi) = -3\varphi^2$ does not pass the $(\gamma_{\text{Timing}}-\dot{\omega}-\dot{P}_b)_{1913+16}$ test.

On the contrary, when $\beta_0 < -5$, we find that the test is never passed even for a vanishingly small α_0 (because the term $\alpha_B \partial \ln I_A / \partial \varphi_0$ blows up). In other words, this binary pulsar rules out all the theories $\beta_0 < -5$, $\alpha_0 = 0$, although they are strictly equivalent to general relativity in weak-field conditions. This illustrates the *qualitative* difference between binary-pulsar and solar-system tests.

Generic tensor-scalar theories can be parametrized by the first two derivatives, α_0 and β_0 , of their coupling function $a(\varphi)$, cf. Eq. (4). It is instructive to plot the constraints imposed by all kinds of tests in the plane (α_0, β_0) . Figure 8 shows that solar-system experiments do not constrain at all the curvature β_0 of $a(\varphi)$ if its slope α_0 is small enough. On the contrary, binary pulsars impose $\beta_0 > -5$, independently of α_0 . Using Eqs. (5b), (5c), this bound can be expressed in terms of the Eddington parameters:

$$\frac{\beta^{\text{PPN}} - 1}{\gamma^{\text{PPN}} - 1} < 1.3 . \quad (14)$$

The singular (0/0) nature of this ratio vividly expresses why such a conclusion could not be obtained in weak-field experiments.

Recent cosmological studies, notably [14], have shown that theories with a positive β_0 are easily consistent with observational data, whereas some

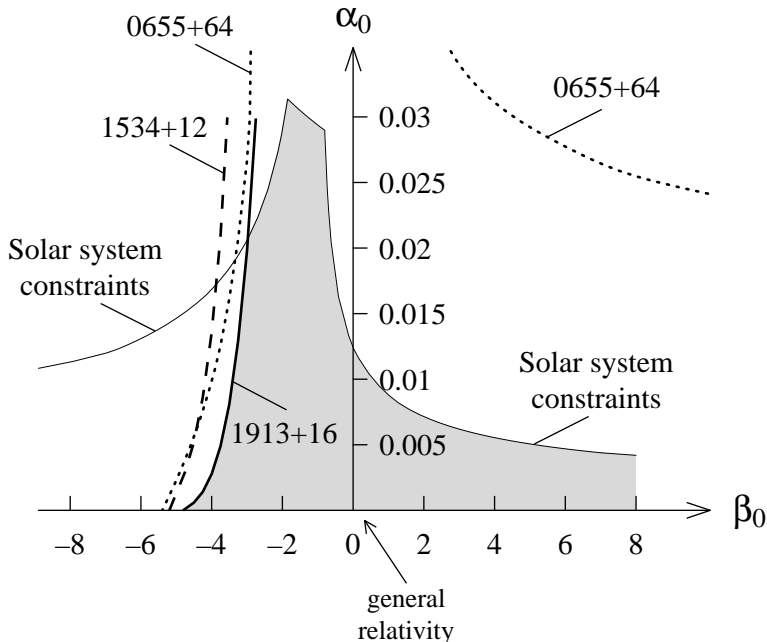


Figure 8: Constraints imposed by solar-system and binary-pulsar experiments in the plane (α_0, β_0) . In view of the reflection symmetry $\alpha_0 \rightarrow -\alpha_0$, only the upper half plane is plotted. The allowed regions are below and on the right of the different curves. The shaded region is allowed by all the tests.

fine-tuning would be required if $\beta_0 < 0$. It is fortunate that binary pulsars precisely privilege the positive values of this parameter.

6 Conclusions

Tensor-scalar theories of gravity are the most natural alternatives to general relativity. They are useful as contrasting alternatives, and can suggest new experimental tests. For instance, the tensor-bi-scalar model of Sec. 4 proved that a single binary-pulsar test does not suffice. Well-behaved tensor-scalar theories (with no negative energy, no large dimensionless parameters, and no fine tuning) can develop nonperturbative strong-field effects analogous to the spontaneous magnetization of ferromagnets. Their study illustrates the qualitative difference between binary-pulsar and solar-system experiments: binary pulsars have the capability of testing theories which are strictly equivalent to general relativity in the solar system.

References

- [1] A.S. Eddington, *The Mathematical Theory of Relativity* (Cambridge University Press, Cambridge, 1923).
- [2] C.M. Will and K. Nordtvedt, *Astrophys. J.* **177**, 757 (1972).
- [3] R.A. Hulse and J.H. Taylor, *Astrophys. J.* **195**, L51 (1975).
- [4] A. Wolszczan, *Nature* **350**, 688 (1991).
- [5] J.H. Taylor, A. Wolszczan, T. Damour, and J.M. Weisberg, *Nature* **355**, 132 (1992).
- [6] T. Damour and G. Schäfer, *Phys. Rev. Lett.* **66**, 2549 (1991).
- [7] N. Wex, gr-qc/9511017, *Astron. Astrophys.*, in press.
- [8] T. Damour and J.H. Taylor, *Phys. Rev D* **45**, 1840 (1992).
- [9] K. Nordtvedt, *Astrophys. J.* **297**, 390 (1985).
- [10] T. Damour and G. Esposito-Farèse, *Class. Quantum Grav.* **9**, 2093 (1992).
- [11] T. Damour and G. Esposito-Farèse, gr-qc/9506063, *Phys. Rev. D* **53**, 5541 (1996).
- [12] T. Damour and G. Esposito-Farèse, gr-qc/9602056, *Phys. Rev. D* **54**, 1474 (1996).
- [13] T. Damour and G. Esposito-Farèse, *Phys. Rev. Lett.* **70**, 2220 (1993).
- [14] T. Damour and K. Nordtvedt, *Phys. Rev. Lett.* **70**, 2217 (1993).